Large-scale climate patterns and precipitation in an arid endorheic region: linkage and underlying mechanism

2016 Environ. Res. Lett. 11 044006

(http://iopscience.iop.org/1748-9326/11/4/044006)

Environmental Research Letters

CrossMark

OPEN ACCESS

RECEIVED
10 November 2015

REVISED
29 February 2016

ACCEPTED FOR PUBLICATION
16 March 2016

PUBLISHED
7 April 2016

LETTER

Large-scale climate patterns and precipitation in an arid endorheic region: linkage and underlying mechanism

Pengfei Shi[1], **Tao Yang**[1,2], **Ke Zhang**[1,3], **Qiuhong Tang**[4], **Zhongbo Yu**[1] **and Xudong Zhou**[1]

[1] State Key Laboratory of Hydrology-Water Resources and Hydraulic Engineering, Center for Global Change and Water Cycle, Hohai University, Nanjing 210098, People's Republic of China
[2] State Key Laboratory of Desert and Oasis Ecology, Xinjiang Institute of Ecology and Geography, Chinese Academy of Sciences, Urumqi, People's Republic of China
[3] Cooperative Institute for Mesoscale Meteorological Studies, University of Oklahoma, Norman, OK 73072, USA
[4] Institute of Geographic Science and Natural Resources Research, Chinese Academy of Sciences, People's Republic of China

E-mail: yang.tao@ms.xjb.ac.cn

Keywords: large-scale climate patterns, climate phases, precipitation, teleconnection, arid endorheic region, amplification effect

Supplementary material for this article is available online

Abstract

The interactions between a range of large-scale climate oscillations and their quantitative links with precipitation are basic prerequisites to understand the hydrologic cycle. Restricted by the current limited knowledge on underlying mechanisms, statistical methods (e.g. correlation methods) are often used rather than a physical-based model. However, available correlation methods generally fail to explain the interactions among a wide range of climate oscillations and associated effects on the water cycle. This study presents a new probabilistic analysis approach by means of a state-of-the-art Copula-based joint probability distribution to characterize the aggregated behaviors for large-scale climate patterns and their connections to precipitation. We applied this method to identify the complex connections between climate patterns (westerly circulation (WEC), El Niño-Southern Oscillation (ENSO) and Pacific Decadal Oscillation (PDO)) and seasonal precipitation over a typical endorheic region, the Tarim River Basin in central Asia. Results show that the interactions among multiple climate oscillations are non-uniform in most seasons and phases. Certain joint extreme phases can significantly trigger extremes (flood and drought) owing to the amplification effect among climate oscillations. We further find that the connection is mainly due to the complex effects of climatic and topographical factors.

1. Introduction

The large-scale atmospheric oscillations are of paramount importance for global or regional water cycle and energy balance (Philips *et al* 2012, Trenberth *et al* 2014) and vegetation (Zhang *et al* 2007), thus have profound impacts on water resources development and hazard prevention and mitigation (Yang *et al* 2014). For example, the record-breaking high global temperature and devastating floods worldwide in 1998 can be partly attributed to El Niño (Lean and Rind 2008, Foster and Rahmstorf 2011), and the 2010 Pakistan flood was linked to a strong La Niña (Coumou and Rahmstorf 2012).

A number of efforts have been implemented to address the impacts from large-scale climate oscillations on the water cycle by using a collection of techniques. Philips *et al* (2012) analyzed the influence of the ENSO on terrestrial water storage using monthly estimates of continental water storage from the Gravity Recovery and Climate Experiment (GRACE). Xu *et al* (2007) identified the relationship between precipitation and ENSO in China by using the non-parametric Kendall's τ. Kim *et al* (2008) developed an influence index to measure the effect of climate variation on precipitation.

Many studies have investigated the atmospheric circulation patterns (e.g. ENSO, PDO) and the associated effects on precipitation, and these studies have detected generally consistent and systematic relationships (Hu and Feng 2001, Van Oldenborgh and Burgers 2005, Timm *et al* 2005, Goodrich 2007, Stevens and Ruscher 2014). However, those atmospheric oscillations are non-independent and collectively affecting over some areas. There

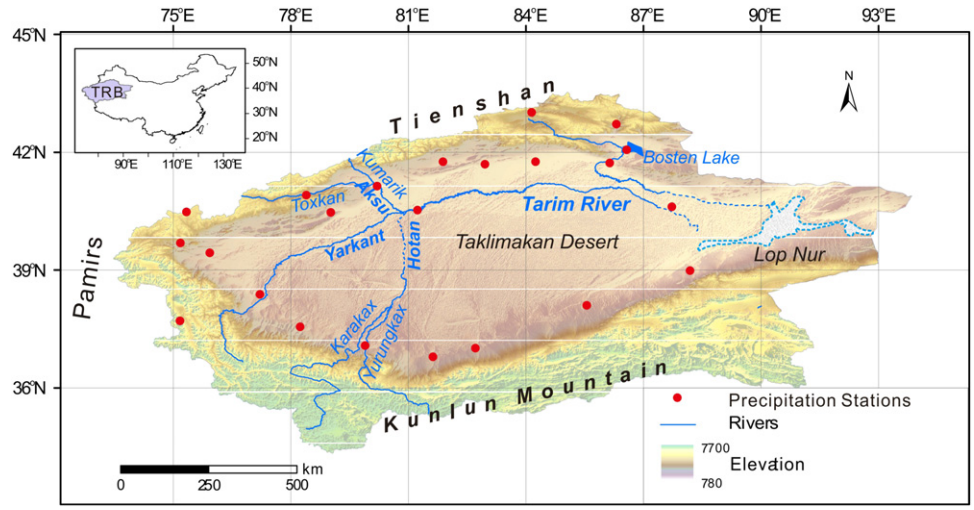

Figure 1. Map of the Tarim River Basin and major precipitation stations.

actually exists intricate interplay among the multiple and large-scale climate oscillations (Steinman *et al* 2014), which constitutes a complex climate–land coupled system, especially in semiarid central Asia. Multiple atmospheric oscillations collectively impose a more complex influence on local precipitation. Restricted by the current limited knowledge on underlying mechanisms, physical-based methodologies generally fail to explain the complex interactions. Thus, statistical methods (e.g. correlation methods) are often used to discover and delineate these complex relationships. However, available statistical methodologies are generally unable to explain the interactions among a wide range of climate oscillations and associated effects on water cycle in some areas around the world (Xu *et al* 2004). To date, identification of dimensional interactions among multiple large-scale circulations and associated hazardous impacts (flood and drought) is still a weak point in global change studies (Boers *et al* 2014). Recently, copulas has been extensively used in high-dimensional probabilistic statistical analysis (Zhang *et al* 2012), providing us a beneficial means to analyze the underlying processes that could not be modeled by current physical based models and described by correlation methods. Copulas are able to characterize the dependence structure independently of the marginal distributions (Genest *et al* 1995, Favre *et al* 2004). It is therefore beneficial to be used in identification for the interactions among non-independent atmospheric oscillations and associated hazardous impacts by means of copula algorithm.

The work strives to: (1) characterize the interplay among multiple large-scale climate oscillations based on joint probability density generated by Copulas; (2) construct a series of climate phases and a quantitative connection based on the phases; (3) address the potential impacts of multiple extreme phases on precipitation and analyze the underlying mechanisms. The Tarim River Basin (34° N–43° N, 73° E–93° E), a typical arid and endorheic region in Central Asia, is selected as study domain to demonstrate the approach. The climate of this region is dominated by the westerly circulation (WEC) and influenced by ENSO and PDO and some other factors (e.g. the Moonsoon and topographical factors) (Chen *et al* 2009, Wu *et al* 2012). WEC represents regional climate pattern, while ENSO and PDO are phenomena of global and hemispheric circulation patterns, respectively. Thus, the three climate patterns and their indices are chosen to represent multiple large-scale climate oscillations that play as major influence on climate in the study region.

2. Methodology

2.1. Data

The observed monthly precipitation data from 23 stations across the basin (figure 1) during 1960–2014 are used in this study and compiled from the China Meteorological Data Sharing Service System (http://cdc.nmic.cn/home.do). Three climate indices, ZI (zonal index), SOI (Southern Oscillation Index) and PDO, are utilized to represent the westerly circulation, ENSO and PDO, respectively. The monthly time series of ZI for the period of 1979–2014 are calculated according to $H_{40^\circ\,\mathrm{N}} - H_{65^\circ\,\mathrm{N}}$, where H is the monthly mean geopotential height in 500 hPa from 73° E to 93° E. The geopotential data is obtained from ERA-Interim Reanalysis data (1° × 1°) (www.ecmwf.int/en/research/climate-reanalysis/era-interim), which is the latest global atmospheric reanalysis produced by the European Centre for Medium-Range Weather Forecasts (ECMWF). The monthly time series of SOI and PDO for the period of 1951–2014 are from the Earth System Research Laboratory, NOAA (www.esrl.noaa.gov/psd/data/climateindices/list/).

2.2. Methodology

We proposed a consolidated framework (figure 2) for new probabilistic analysis approach by means of a

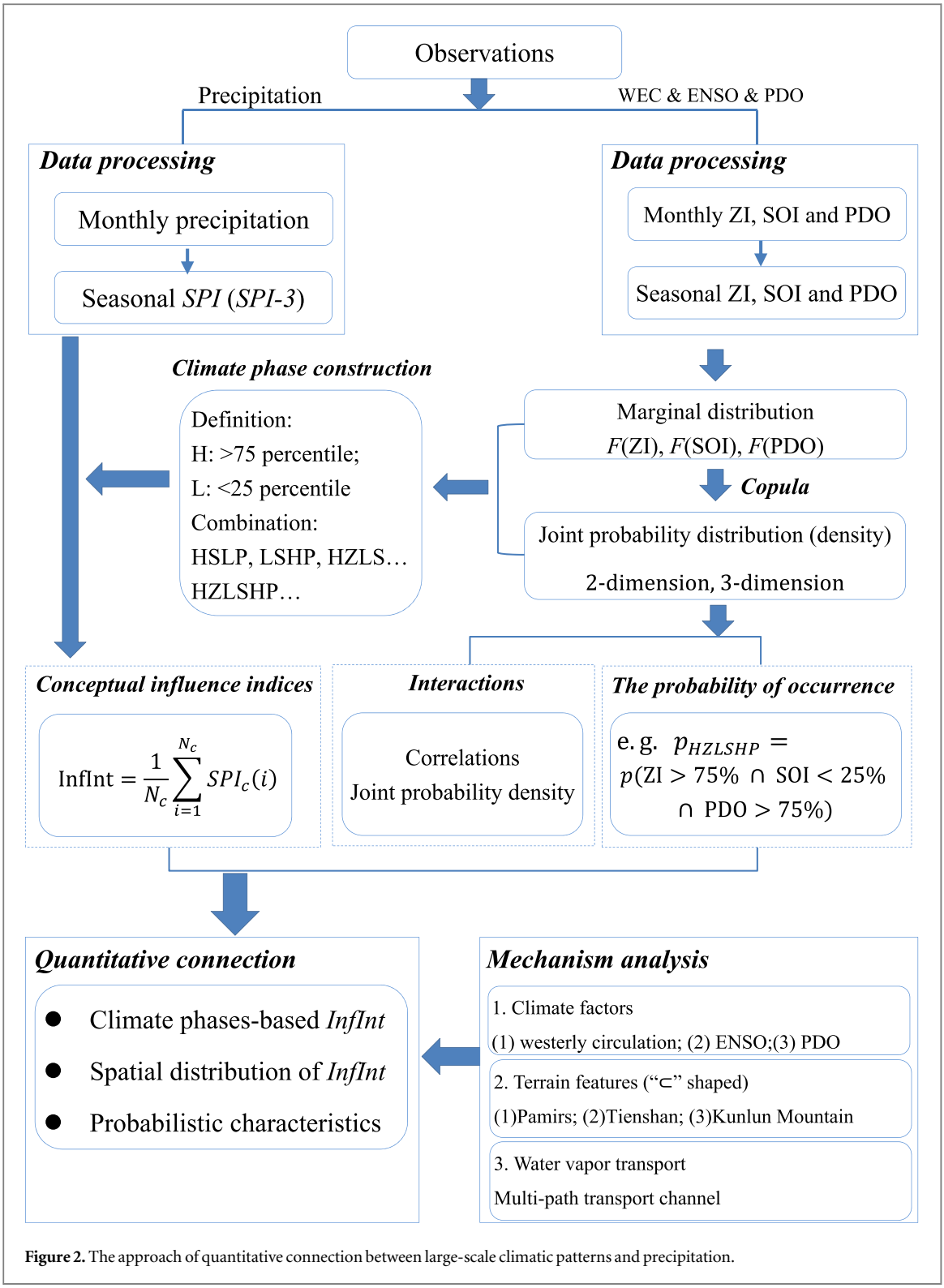

Figure 2. The approach of quantitative connection between large-scale climatic patterns and precipitation.

state-of-the-art Copula-based joint probability distribution to characterize the aggregated behaviors for large-scale climate patterns and their connections to precipitation. It includes three steps: (1) construct a multivariate joint probability distribution based on three marginal distributions of large-scale climate indices to characterize interplay; (2) build a series of conceptual influence indices according to the Copula-based joint probabilistic phases and standardized precipitation index (SPI); and (3) conduct a composite mechanism analysis for further verifying the connection. The joint distribution is expressed as follows:

$$P = \begin{cases} F(X) & \text{marginal distribution} \\ F(U, V, Z) & \text{three-dimensional joint distribution} \end{cases} \quad (1)$$

where P represents the probability distributions, U, V and Z represent climatic indices (i.e. ZI, SOI and PDO), and X can be each of them. According to the fitted

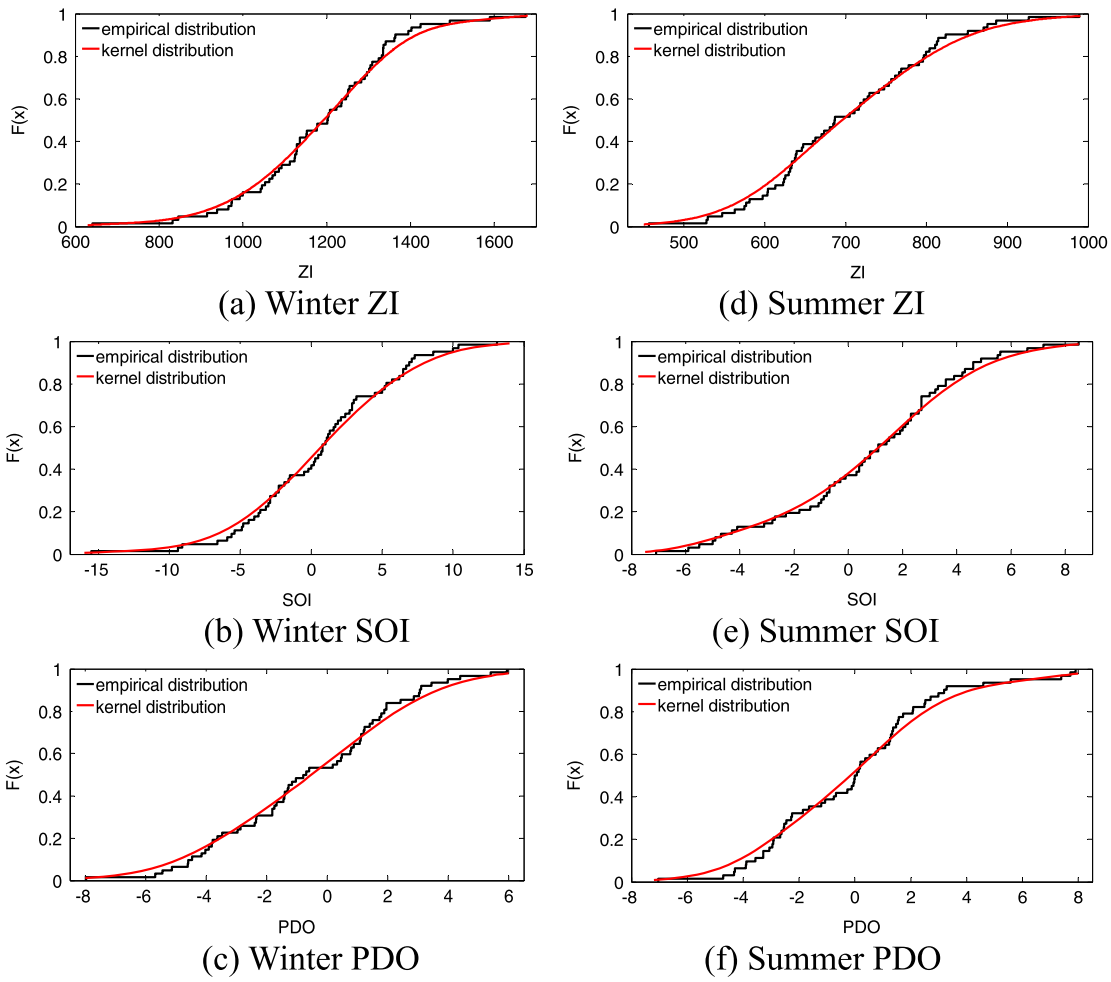

Figure 3. Marginal probability distributions for ZI, SOI and PDO.

marginal probability distributions (figure 3) and dual joint probability densities (figures 4 (c)–(h)), we define that the seasonal climate indices larger than 75 percentile is high phase and smaller than 25 percentile is low phase. Then these single phases are aggregated together to generate a series of dual and triple joint phases (table 1). The corresponding occurrence probabilities of these phases (e.g. $p_{HZLSHP} = p(\mathrm{ZI} > 75 \text{ percentile} \cap \mathrm{SOI} < 25 \text{ percentile} \cap \mathrm{PDO} > 75 \text{ percentile})$ are obtained (table1) through integration for the joint probability density function. In order to investigate the quantitative links between these phases and precipitation, an influence intensity index (InfInt) was used to quantify the strength of teleconnections (Kim *et al* 2006):

$$\mathrm{InfInt} = \frac{1}{N_c}\sum_{i=1}^{N_c} SPI_c(i) \qquad (2)$$

where N_c is the number of years of a climate phase, and $SPI_c(i)$ is the seasonal SPI corresponding to year i. The *SPI* quantifies observed precipitation as a standardized departure from a selected probability distribution function that models the raw precipitation data (McKee *et al* 1993). It has zero mean and unit standard deviation and provides a measure of the precipitation frequency distribution. In addition, the *SPI* has an advantage to capture multi-temporal nature of rainfall deficiency and is usually computed for a certain time interval (monthly or seasonally). InfInt can be interpreted by the moisture classification shown in table 2 (Mckee *et al* 1993, Kim *et al* 2006, National Climate Center, China).

3. Results

Two seasons are included in this study: summer (June, July and August) and winter (December, January and February). The two seasons (summer and winter) are chosen due to that these two seasons are two extremes (maximum and minimum) in terms of the amount of precipitation. There are less precipitation extremes in spring and autumn over the region. The probability distributions (density) (figure 4) are constructed to characterize the geostatistical interactions among multiple climate oscillations.

3.1. The interplay of multi-source large-scale climatic patterns

For characterizing the multivariate non-independent climatic variables, we used statistical technique rather

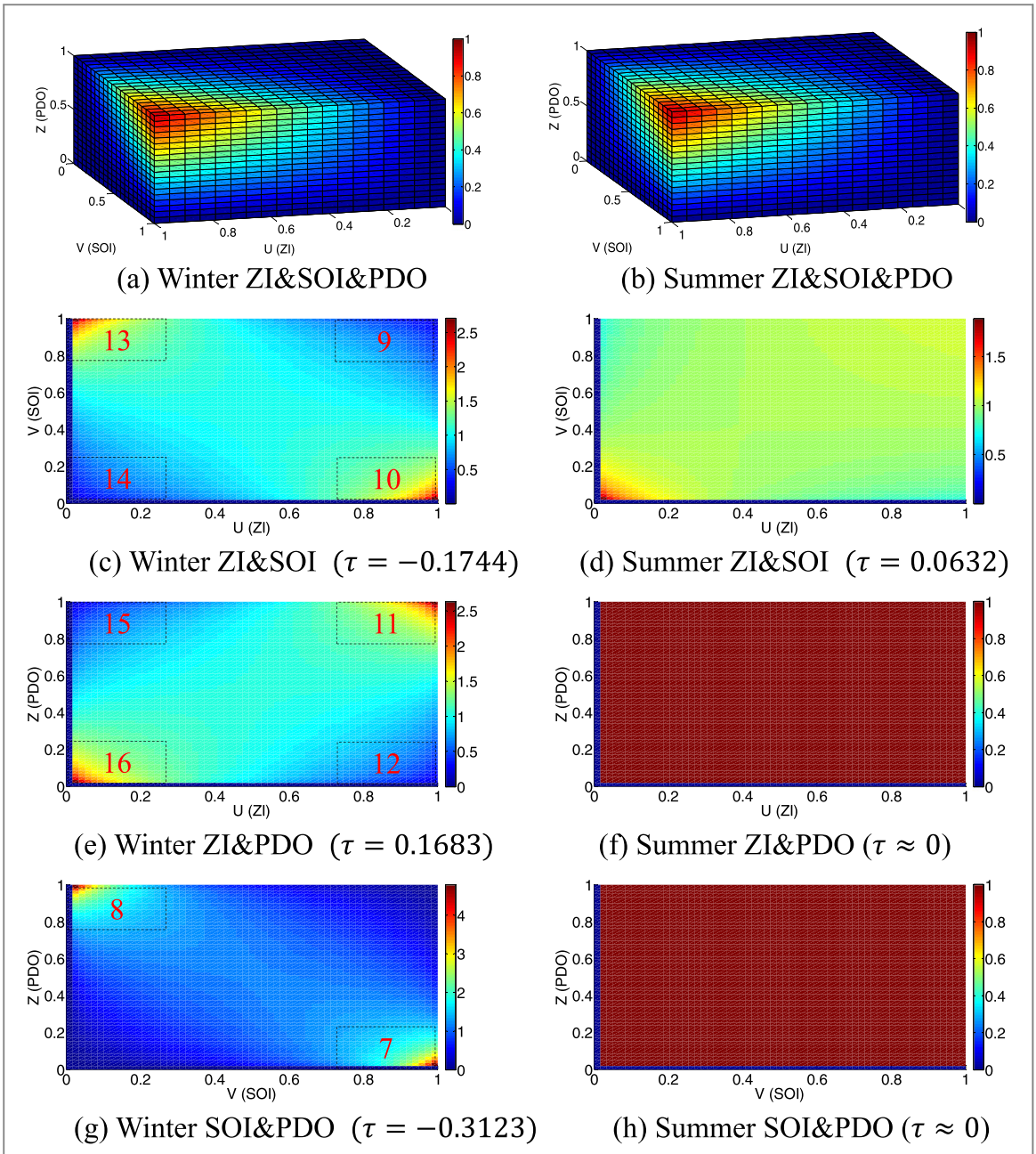

Figure 4. Three-dimensional joint probability distribution for ZI, SOI and PDO (a)–(b). Two-dimensional joint probability density (c)–(h). Note: the marginal probability density is normalized to uniform by Copula; the joint probability (density) are denoted by color; τ denotes the rank correlation coefficient; these numbers in red denote the climate phases listed in table 1.

than the physical based methods. Firstly, we use a kernel density function to estimate the marginal distribution of seasonal ZI, SOI and PDO (figure 3). Then, a series of commonly used copula functions (Gaussian, Clayton, Frank and Gumbel Copula) are used to construct joint probability distribution for the three indices. Akaike's information criterion (AIC) and Euclidean distance are employed to identify the appropriate function (table 3). Small values of the two measures suggest good fit (Akaike 1974). The fitted three-dimensional joint probability distribution is shown in figures 4(a)–(b). According to the fitted joint probability distribution, we extract the two-dimensional probability density (figures 4(c)–(h)) to analyze the combining characteristic so as to reveal the interplay among them. The joint probability densities for climatic indices show different characteristics. In winter, the joint probability density of ZI and SOI shows that the two climate patterns tend to appear in opposite phases (figure 4(c)). In other words, the probability density is high when one of the two climate patterns has a low phase and the other has a high phase, and is low when both climate patterns have the same phases. Similar characteristics exist in the probability density for SOI and PDO (figure 4(g)). On the contrary, ZI and PDO appear to have consistent phases (figure 4(e)). Generally, the multiple large-scale climatic patterns are correlated with each other to some degree in winter, especially during the extreme phases (figures 4(c), (e), (g)). In summer, correlations are not

Table 1. A series of large-scale climate phases.

No.	Climate phases	Definition	Calculation	Probability	
				Summer	Winter
1	HZ	Years with high ZI	$SCI_{(ZI)} > 75$ percentile		
2	LZ	Years with low ZI	$SCI_{(ZI)} < 25$ percentile		
3	HS	Years with high SOI	$SCI_{(SOI)} > 75$ percentile		
4	LS	Years with low SOI	$SCI_{(SOI)} < 25$ percentile		
5	HP	Years with high PDO	$SCI_{(PDO)} > 75$ percentile		
6	LP	Years with low PDO	$SCI_{(PDO)} < 25$ percentile		
7	HSLP	HS & LP	$SCI_{(SOI)} > 75$ percentile & $SCI_{(PDO)} < 25$ percentile	5.06%	8.51%
8	LSHP	LS & HP	$SCI_{(SOI)} < 25$ percentile & $SCI_{(PDO)} > 75$ percentile	5.06%	8.51%
9	HZHS	HZ & HS	$SCI_{(ZI)} > 75$ percentile & $SCI_{(SOI)} > 75$ percentile	5.38%	2.97%
10	HZLS	HZ & LS	$SCI_{(ZI)} > 75$ percentile & $SCI_{(SOI)} < 25$ percentile	4.61%	6.68%
11	HZHP	HZ & HP	$SCI_{(ZI)} > 75$ percentile & $SCI_{(PDO)} > 75$ percentile	5.06%	6.60%
12	HZLP	HZ & LP	$SCI_{(ZI)} > 75$ percentile & $SCI_{(PDO)} < 25$ percentile	5.06%	3.04%
13	LZHS	LZ & HS	$SCI_{(ZI)} < 25$ percentile & $SCI_{(SOI)} > 75$ percentile	4.61%	6.68%
14	LZLS	LZ & LS	$SCI_{(ZI)} < 25$ percentile & $SCI_{(SOI)} < 25$ percentile	5.72%	2.97%
15	LZHP	LZ & HP	$SCI_{(ZI)} < 25$ percentile & $SCI_{(PDO)} > 75$ percentile	5.06%	3.04%
16	LZLP	LZ & LP	$SCI_{(ZI)} < 25$ percentile & $SCI_{(PDO)} < 25$ percentile	5.06%	6.60%
17	HZHSLP	HZ & HS & LP	$SCI_{(ZI, SOI)} > 75$ percentile & $SCI_{(PDO)} < 25$ percentile	2.23%	0.98%
18	HZLSHP	HZ & LS & HP	$SCI_{(ZI, PDO)} > 75$ percentile & $SCI_{(SOI)} < 25$ percentile	1.78%	3.26%
19	LZHSLP	LZ & HS & LP	$SCI_{(ZI, PDO)} < 25$ percentile & $SCI_{(SOI)} > 75$ percentile	1.64%	3.26%
20	LZLSHP	LZ & LS & HP	$SCI_{(ZI, SOI)} < 25$ percentile & $SCI_{(PDO)} > 75$ percentile	2.34%	0.98%

Note: *SCI* denotes the seasonal climate indices (i.e. the annual time series of the sum of monthly climate indices during a season). Not all combined phases are listed here, as some of which do not appear in the observation.

Table 2. SPI, cumulative probability and their corresponding moisture classification.

SPI	CDF	
−3.0	0.001	
−2.5	0.006	
−2.0	0.023	Extreme dry (ED)
−1.5	0.067	Severe dry (SD)
−1.0	0.159	Moderate dry (MD)
−0.5	0.309	Incipient dry (ID)
0	0.500	Nearly normal (NN)
0.5	0.691	Incipient wet (IW)
1.0	0.841	Moderate wet (MW)
1.5	0.933	Severe wet (SW)
2.0	0.977	Extreme wet (EW)
2.5	0.944	
3	0.999	

as obvious as that in winter. Only ZI and SOI show notable correlation in the down tail (figure 4(d)). There are almost no correlation between ZI and PDO (figure 4(f)) and between SOI and PDO (figure 4(h)). Till far, the complex interplay of the climate oscillations is identified based on the probabilistic approach.

3.2. Climate phases-based analysis of influence intensity

InfInt for 23 stations are aggregated as box plots (figures 5(a), (c)) to reveal the effects of different climate phases. The box-plots presented in figure 5(a) show the influence intensity for 20 climate phases in summer. The median values in the separate climate phases (No. 1–6, table 1) are both between 0.5 and −0.5, indicating the phase of any of the three climate oscillations does not strongly associate with drought and wetness in these regions. InfInt during joint climate phases seem to be more dynamic and greater than that during the separate ones. To interpret InfInt during joint phases, we compare the values during joint phases that include the same term. Through comparisons, we find that ENSO has obvious wet effect during the high phase of PDO (i.e. LSHP) and the effect almost disappears during the low phase of PDO (i.e. HSLP). It implies that PDO has regulation roles in ENSO. The westerly wind brings disturbances to the region. However, the role of westerly wind is not consistent. High phase of westerly wind sometimes enhances the wetness (i.e. HZLS) and sometimes counteracts wetness (or makes dry effect) (i.e. HZLSHP, HZHSLP), and low phase makes wet effect (i.e. LZHS, LZHP). Generally, it can be concluded that the phases LS and LZ seem to make wet effects and these influences only take effect during the joint climate phases. An amplification effect by high phase of other climate indices is found. That is to say, single climate phases with wet effect often seem to be dormant when not accompanied by the high phases of the other climate oscillations, but come alive when coincide with high phases of other climate patterns. The joint effects of two low phases are almost useless and two high phases together often trigger drought. In winter, the picture (figure 5(c)) is different comparing with that for summer. The joint effect of ENSO and PDO is not obvious. The single phase LS makes the

Table 3. AIC and Euclidean distance for different copula functions.

	Euclidean distance AIC value			
	Normal Copula	Clayton Copula	Frank Copula	Gumbel Copula
Summer	0.0470	**0.0321**	0.0357	0.0336
	−442.4797	***−465.9933***	−459.4976	−463.1640
Winter	**0.0303**	0.0688	0.0406	0.0688
	-469.6832	−418.8027	−451.4714	−418.8023

Note: Values in bold and italics means the best, thereby the corresponding function is selected to fit the joint probability distribution.

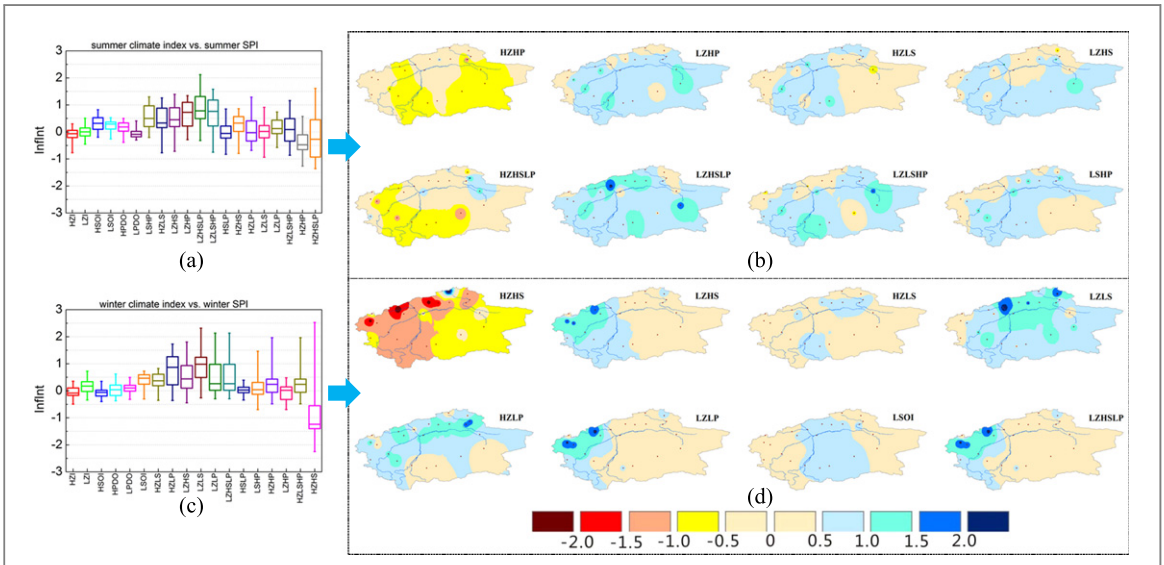

Figure 5. Influence intensity for summer (a), (b) and winter (c), (d) precipitation. Note: The box plots show the minimum (lower cap), maximum (upper cap), median (line in the box), lower (bottom of the box) and upper (top of the box) quartiles of data.

region partly wet. Lower phases of atmospheric oscillation (LP, LZ and LS) seem to help the formation of precipitation in region, but it still, or at least partly, rely on the influences from other climate patterns. Different to that in summer, there is no consistent, basin-wide amplification effect by the combinations of high or low phases of these climate oscillations. What can be determined is that two high phases together often trigger drought (e.g. HZHS). It implies that the strong west wind together with strong atmospheric oscillation go against the concentration of warm water vapor and formation of precipitation in winter.

We select 8 typical climate phases with conspicuous effects to show the spatial distributions of influence intensity (figures 5(b), (d)). In summer, incipient dry (ID) dominates in the upper basin (western part, Yarkant River and Hotan River) and lower basin (eastern and southeast part) during HZHP, and prevails in the upper basin (western part, Yarkant River and Hotan River) and southern part of the region during HZHSLP (figure 5(b)). Incipient dry (ID) condition appears during the double-combined climate phases including 'HZ', whereas wet conditions (incipient wet, moderate wet) emerge during all climate phases including 'LZ' and 'LS'. In winter (figure 5(d)), dry conditions dominate almost over the whole basin during HZHS, western half and eastern half of which are controlled by moderate dry (MD) and incipient dry (ID), respectively. The last 6 phases both make the basin wet more or less.

In general, certain phases have been proved to be highly related to hydrologic extremes (flood and drought). Meanwhile, the occurrence probabilities of these joint extreme phases (table 1) are not low. Therefore, these joint extreme phases are worthy of more attention in water resources and agriculture management in this arid region.

4. Discussions

Wu *et al* (2012) simulated the annual average water vapor transport and identified the transportation routes over the Tarim River Basin. Based on the simulation results, we drew a conceptual, theoretical schematic graph (figure 6) to compendiously show the water vapor transportation and correspondingly to explain the linkages between different climate

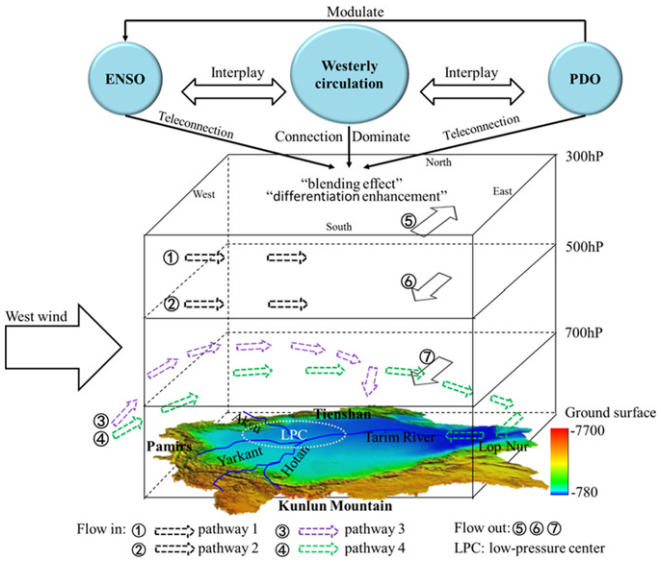

Figure 6. The interplay of large-scale climate patterns and the schematic diagram of water vapor transport in Tarim River Basin.

oscillations and precipitation pattern. The basin is located at the peculiar location with complicated climatic and topographic conditions, it is likely that this water vapor exchange depends on the joint effect of large scale climate patterns (i.e. westerly circulation, ENSO, PDO and so on) and the specific '⊂' shaped terrain back to west wind. In details, the westerly circulation prevails at the upper layer (500hP to 300hP) of troposphere and brings water vapor into the basin (path 1, marked as ① in figure 6), and weakens at the middle layer (path 2, marked as ②) due to the influence from altitude of Qinghai-Tibet Plateau and monsoon. At the lower layer, the specific '⊂' shaped terrain significantly influences the water vapor transport. Water vapor could not been transported to the basin from the west boundary and south boundary at the lower layer of troposphere owing to the hindrance of Pamir (average elevation: 4000–7700 m) and Kunlun mountain (average elevation: 5500–6000 m). Some airflow swerves northward and flows to the basin from the northern (Tienshan, average elevation: about 3000 m) via path 3 (marked as ③). Additionally, a low-pressure center (shown as LPC) at the middle and lower layer of troposphere exists over basin because of that the strong westerly circulation at the upper layer acts as 'pumping' over the '⊂' shaped terrain. Thereby, a large amount of airflow swerves and flows to the basin from the east boundary (average elevation: about 1000 m) via path 4 (marked as ④). Airflow flows out of the basin from the northern boundary at upper layer (marked as ⑤), and from the southern boundary at upper (marked as ⑥) and middle layer (marked as ⑦).

According to the water vapor transport over the basin, we further interpret the linkage between different climate oscillations and precipitation pattern. In summer, most water vapor input comes from the east, west and north boundaries, especially the east owing to the existence of LPC. It is likely owing to that the west wind is weaker in summer thus the height of LPC is low, thereby indraft appears from the east. The large water vapor from east at lower position helps the formation of precipitation. This partly explains why wet conditions emerge during all climate phases including the 'LZ' phases (LZHP, LZHSLP, LZLSHP and LZHS) in summer (figure 5(b)). On the contrary, strong west wind brings water vapor from high layer, which prevents the formation of precipitation. This probably explains why the 'HZ' phases (HZHP, HZHSLP) lead to dry effect (figure 5(b)). The west wind in winter is strong and at higher layer, which count against the accumulation of water vapor. The strong west wind together with strong atmospheric oscillation (i.e. HZHS) causes the region dry in winter (figure 5(d)). Though the respective exact contribution of westerlies and terrain to the precipitation regime remain elusive, what's undoubtedly is that there exists specific multi-path water vapor channels and the westerly wind affects the precipitation regime in the basin.

ENSO and PDO represent the anomalies of sea level pressure and sea surface temperature, respectively (Ropelewski and Halpert 1986, Hare and Mantua 2001). Thus, it is undoubtedly that ENSO together with PDO can affect the prevailing intrinsic climate (dominated mostly by westerlies and terrain) and thereupon influence the water vapor transportation more or less. This influence is probably just a modulation or a disturbance, but it indeed has important impacts on precipitation. Additionally, the El Niño events (low phase of SOI) brings warm and wet air therefore influence the precipitation in the basin. This can partly explain why wet conditions emerge during the climate phases including 'LS'. Furthermore, PDO has obvious regulation roles on some other climate

oscillations (Hu and Feng 2001). In winter, low phase of PDO probably helps make the region wet. In other words, most of the climate phases including 'LP' make the region wet (figure 5(d)). However, this regulation role is not consistent in summer. Extremes emerge both under the climate phases including 'HP' and 'LP'. It is probably because that PDO has no correlation with ZI and SOI in summer (figures 4(f), (h)). The underlying mechanisms need to be further investigated in the future.

The above deductive qualitative linkages between Westerlies & ENSO & PDO and precipitation are just quantitatively identified in this article by a probabilistic phases- based comprehensive analysis. The inferred qualitative linkage and the quantitative linkage were auxiliary to each other. We further test the method by using combined phases that are neither high nor low. The InfInt during these combined phases indicate nearly normal (NN) both in winter and in summer (figure S1). We can further conclude that extremes (flood and dry condition) are mostly triggered by the combined extreme climate phases, rather than normal phases. It is worth pointing out that the InfInt represents average influence intensity from a certain climate phase. Dry and wet spells still emerge in these normal combined phases, but the average dry-wet condition in the period is normal. In other words, transient wet or dry conditions may appear in certain periods of a climate phase, but the climate phase makes the region nearly normal as a whole.

A physical model (e.g. a global circulation model or regional circulation model) usually generates precipitation by considering some regional and global climate oscillations and some other large-scale climate factors. It is not the best and direct way to detect teleconnections between climate oscillations and precipitation. To the best of our knowledge, there is almost no a physical model that is able to capture all complicated teleconnections, thus statistical techniques (e.g. correlation methods) are usually used instead to detect the complex, multiple linkages or relationships between climate oscillations and precipitation (Cayan *et al* 1999, Lyon and Barnston 2005). However, the traditional correlations methods are not sophisticated enough to investigate the interplay of multiple climate oscillations, which restrict the discovery and quantification of the potential impacts of multiple extreme phases on precipitation (Piechota and Dracup 1996, Xu *et al* 2004). The Copula-based joint probability distribution constructed in this article has disclosed the intricate interplay among the multiple and large-scale climate oscillations, which is not revealed by previous study (Kim *et al* 2006). In addition, the complex effect of multiple climate oscillations on precipitation is successfully delineated by using the new probabilistic analysis approach, which is also not revealed by previous study investigating the same area (Chen *et al* 2009). They are of importance for understanding the intricate behaviors of large-scale climatic patterns on local precipitation, thus have profound impacts on water resources development and hazard prevention and mitigation over the arid and inland zone.

5. Conclusions

In this work, a new probabilistic analysis approach by means of a state-of-the-art Copula-based joint probability distribution is constructed to characterize the aggregated behaviors for large-scale climate patterns and their connection to precipitation. The intricate interplay among the multiple and large-scale climate oscillations and their connection with precipitation has been successfully detected and identified through the new probabilistic analysis approach. The mechanism analysis of the complex effect derived from climatic and topographical factors explained the connection to a certain degree. These collectively constitute the distinctive deliverables to provide beneficial insights in understanding the intricate behaviors of large-scale climatic patterns on local precipitation over the arid and inland zone.

Results reveal that the response of precipitation to westerly circulation, ENSO and PDO is connected to different seasons and phases. The drought and wetness significantly correlate to the assembled climate phases based on a multivariate Copula analysis. It is the joint extreme phases instead of a single separate phase or joint normal phases trigger different drought and wetness. This depends on the enhancement from other climate phase, and this amplification effect is distinct in summer and winter. The effect has not been revealed in previous studies, but effectively discovered in this study by means of a consolidated probabilistic analysis. The technique can be widely applied to address teleconnections of multivariate large scale climate patterns with droughts and floods in other regions worldwide.

Acknowledgments

The work was jointly supported by a grant from the National Natural Science Foundation of China 41371051, a key grant of Chinese Academy of Sciences KZZD-EW-12, a grant from the Ministry of Science and Technology of China 2013BAC10B01 and grants from the Fundamental Research Funds for the Central Universities 2015B25714, 2014B34514, and 2015B28514.

References

Akaike H 1974 A new look at the statistical model identification *IEEE Trans. Autom. Control* **AC-19** 716–23

Boers N, Bookhagen B, Barbosa H M J, Marwan N, Kurths J and Marengo J A 2014 Prediction of extreme floods in the eastern Central Andes based on a complex networks approach *Nat. Commun.* **5** 5199

Cayan D R, Redmond K T and Riddle L G 1999 ENSO and hydrologic extremes in the western United States* *J. Clim.* **12** 2881–93

Chen Y, Xu C, Hao X, Li W, Chen Y, Zhu C and Ye Z 2009 Fifty-year climate change and its effect on annual runoff in the Tarim River Basin, China *Quaternary International* **208** 53–61

Coumou D and Rahmstorf S 2012 A decade of weather extremes *Nat. Clim. Change* **2** 491–6

Favre A C, El Adlouni S, Perreault L, Thiémonge N and Bobée B 2004 Multivariate hydrological frequency analysis using copulas *Water Resour. Res.* **40** W01101

Foster G and Rahmstorf S 2011 Global temperature evolution 1979–2010 *Environ. Res. Lett.* **6** 044022

Genest C, Ghouci K and Rivest L P 1995 A semiparametric estimation procedure of dependence parameters in multivariate families of distributions *Biometrika* **82 543–52**

Goodrich G B 2007 Influence of the pacific decadal oscillation on winter precipitation and drought during years of neutral ENSO in the western United States *Weather and Forecasting* **22** 116–24

Hare S R and Mantua N J 2001 An historical narrative on the Pacific Decadal Oscillation, interdecadal climate variability and ecosystem impacts *CIG Publication No* University of Washington, Seattle, WA

Hu Q and Feng S 2001 Variations of teleconnection of ENSO and interannual variation in summer rainfall in the central United States *J. Clim.* **14** 2469–80

Kim T W, Valdes J B, Nijssen B and Roncayolo D 2006 Quantification of linkages between large-scale climatic patterns and precipitation in the Colorado River Basin *J. Hydrol.* **321** 173–86

Kim T W, Yoo C and Ahn J H 2008 Influence of climate variation on seasonal precipitation in the Colorado River Basin *Stoch. Environ. Res. Risk. Assess* **22** 411–20

Lean J L and Rind D H 2008 How natural and anthropogenic influences alter global and regional surface temperatures: 1889 to 2006 *Geophys. Res. Lett.* **35** 1–6

Lyon B and Barnston A G 2005 ENSO and the spatial extent of interannual precipitation extremes in tropical land areas *J. Clim.* **18** 5095–109

McKee T B, Doesken N J and Kleist J 1993 The relationship of drought frequency and duration to time series *8th Conf. on Applied Climatology* (*Anaheim, CA*) *1993*, pp 179–87

National Climate Center, China (http://cmdp.ncc-cma.net/extreme/dust.php?product=dust_moni)

Phillips T, Nerem R S, Fox-Kemper B, Famiglietti J S and Rajagopalan B 2012 The influence of ENSO on global terrestrial water storage using GRACE *Geophys. Res. Lett.* **39** L16705

Piechota T C and Dracup J A 1996 Drought and regional hydrologic variation in the united states: associations with the El Niño-Southern Oscillation *Water Resour. Res.* **32** 1359–73

Ropelewski C F and Halpert M S 1986 North American precipitation and temperature patterns associated with the El Niño/Southern Oscillation (ENSO) *Mon. Weather Rev.* **114** 2352–62

Steinman B A, Abbott M B, Mann M E, Ortiz J D, Feng S, Pompeani D P, Stansell N D, Anderson L, Finney B P and Bird B W 2014 Ocean-atmosphere forcing of centennial hydroclimate variability in the Pacific Northwest *Geophys. Res. Lett.* **41** 2553–60

Stevens K A and Ruscher P H 2014 Large scale climate oscillations and mesoscale surface meteorological variability in the Apalachicola-Chattahoochee-Flint River Basin *J. Hydrol.* **517** 700–14

Timm O, Pfeiffer M and Dullo W C 2005 Nonstationary ENSO-precipitation teleconnection over the equatorial Indian Ocean documented in a coral from the Chagos Archipelago *Geophys. Res. Lett.* **32** L02701

Trenberth K E, Dai A, van der Schrier G, Jones P D, Barichivich J, Briffa K R and Sheffield J 2014 Global warming and changes in drought *Nat. Clim. Change* **4** 17–22

Van Oldenborgh G J and Burgers G 2005 Searching for decadal variations in ENSO precipitation teleconnections *Geophys. Res. Lett.* **32** L15701

Wu Y, Shen Y and Li B L 2012 Possible physical mechanism of water vapor transport over Tarim River Basin *Ecological Complexity* **9** 63–70

Xu Z X, Chen Y N and Li J Y 2004 Impact of climate change on water resources in the Tarim River basin *Water Res. Manag.* **18** 439–58

Xu Z X, Li J Y, Takeuchi K and Ishidaira H 2007 Long-term trend of precipitation in China and its association with the El Niño-southern oscillation *Hydrol. Process.* **21** 61–71

Yang T, Wang X, Yu Z, Krysanova V, Chen X, Schwartz F W and Sudicky E A 2014 Climate change and probabilistic scenario of streamflow extremes in an alpine region *J. Geophys. Res.: Atmos.* **119** 8535–51

Zhang K, Kimball J S, McDonald K C, Cassano J J and Running S W 2007 Impacts of large-scale oscillations on pan-Arctic terrestrial net primary production *Geophys. Res. Lett.* **34** L21403

Zhang Q, Li J and Singh V P 2012 Application of Archimedean copulas in the analysis of the precipitation extremes: effects of precipitation changes *Theor. Appl. Climatol.* **107** 255–64